Study of excited nucleon states at EBAC: status and plans[*]

Hiroyuki Kamano[1)]

(Excited Baryon Analysis Center (EBAC), Thomas Jefferson National Accelerator Facility, Newport News, VA 23606, USA)

Abstract   We present an overview of a research program for the excited nucleon states in Excited Baryon Analysis Center (EBAC) at Jefferson Lab. Current status of our analysis of the meson production reactions based on the unitary dynamical coupled-channels model is summarized, and the N* pole positions extracted from the constructed scattering amplitudes are presented. Our plans for future developments are also discussed.

Key words   dynamical coupled-channels analysis, meson production reactions, N* pole positions

PACS   13.75.Gx, 13.60.Le, 14.20.Gk

1   Introduction

Understanding the structure of hadrons and their excitations still remains as an outstanding and fundamental challenge in the hadron physics. The existence of the hadrons is a direct consequence of the confinement of quarks and gluons within the quantum chromodynamics (QCD). Thus exploring the hadron structure is nothing but making clear the nonperturbative nature of QCD.

Recent experimental activities at electron-beam facilities such as JLab, Bonn, Mainz, SPring-8, and GRAAL have brought new light to the study of excited nucleon (N*) states[1]. Those facilities provide a considerable amount of precise data of the meson photo- and electro-production reactions on the nucleon target, and open a great opportunity to make quantitative investigations of the N* structure.

Against the background of those experimental progress, continuous effort to extract the N* properties from the world data of meson production πN, γN, and N(e, e$'$) reactions is being made in Excited Baryon Analysis Center (EBAC) at Jefferson Lab. The analysis is pursued with a dynamical coupled-channels (DCC) approach proposed in Ref. [2]. The approach treats most relevant unitary cuts below $W = 2$ GeV,

i.e., πN, ηN, and $\pi\pi$N which has unstable $\pi\Delta$, ρN, σN channels, in solving the coupled-channels equations.

The objective of EBAC is more than just performing the partial-wave analysis of the meson production reactions. We not only try to extract the N* parameters, but also to map out the quark-gluon substructure of the N* states. It will require comprehensive study combined with various hadron structure calculations such as constituent quark models, covariant models based on Dyson-Schwinger equations, and Lattice QCD simulations. The N* information extracted from the reaction model analysis, such as that performed in EBAC, is vital for bridging the gap between the actual reaction data and the hadron structure calculations.

The main subjects in EBAC are summarized as follows:

1. Establish baryon spectrum.

2. Extract N* parameters, in particular the electromagnetic N-N* transition form factors, from analyzing the world data of meson production πN, γN, N(e, e$'$) reactions.

3. Develop a method to connect the extracted form factors to the hadron structure calculations and deduce the structure of the N* states.

In this paper we present an overview of current

status and future plans of the EBAC program. In Sec. 2 we briefly explain a framework of the EBAC-DCC model, and present the results of our analysis of the meson production reactions in Sec. 3. In Sec. 4 we present the extracted N* pole positions within the current EBAC-DCC model. Finally we discuss our future plan in Sec. 5.

2　EBAC-DCC model

The EBAC-DCC analysis is based on a multi-channels and multi-resonances model[2] within which the partial wave amplitudes of $M(\vec{p}) + B(-\vec{p}) \to M'(\vec{p}') + B'(-\vec{p}')$ are calculated from the following coupled-channels integral equation (suppressing the angular momentum and isospin indices):

$$T_{\mathrm{MB,M'B'}}(p,p';E) = V_{\mathrm{MB,M'B'}}(p,p';E) +$$
$$\sum_{\mathrm{M''B''}} \int_0^\infty \mathrm{d}q\, q^2 V_{\mathrm{MB,M''B''}}(p,q;E) \times$$
$$G_{\mathrm{M''B''}}(q;E) T_{\mathrm{M''B'',M'B'}}(q,p';E). \quad (1)$$

Here $V_{\mathrm{MB,M'B'}}$ and G_{MB} are the MB $\to$ M'B' transition potential and the MB Green function described below; the summation over M''B'' represents the coupled-channels effects among the πN, ηN, $\pi\Delta$, ρN, σN channels in the reaction processes. It is well known that the solution of the above equation automatically satisfies the unitary conditions for the scattering amplitudes.

The MB $\to$ M'B' transition potential is defined as

$$V_{\mathrm{MB,M'B'}}(p,p';E) = v_{\mathrm{MB,M'B'}}(p,p') +$$
$$\sum_{\mathrm{N}_i^*} \frac{\Gamma^\dagger_{\mathrm{N}_i^*,\mathrm{MB}}(p)\Gamma_{\mathrm{N}_i^*,\mathrm{M'B'}}(p')}{E - m^0_{\mathrm{N}_i^*}}, \quad (2)$$

where $m^0_{\mathrm{N}_i^*}$ and $\Gamma^\dagger_{\mathrm{N}_i^*,\mathrm{MB}}(p)$ represent the bare mass of the ith N* state and the bare N$_i^*$ $\to$ MB decay vertex, respectively. The meson exchange potential $v_{\mathrm{MB,M'B'}}$ is derived using the unitary transformation method[3, 4] from phenomenological Lagrangians which respects gauge and chiral symmetries. It is noted that the derived potential is independent of the total scattering energy E. The second term describes a MB $\to$ M'B' transition through the propagation of the bare N* state, MB $\to$ N* $\to$ M'B'. Also, defining $E_\alpha(k) = [m_\alpha^2 + k^2]^{1/2}$ with m_α being the mass of particle α, the meson-baryon propagators in Eq. (1) are $G_{\mathrm{MB}}(k,E) = 1/[E - E_{\mathrm{M}}(k) - E_{\mathrm{B}}(k) + \mathrm{i}\epsilon]$ for the stable πN and ηN channels, and $G_{\mathrm{MB}}(k,E) = 1/[E - E_{\mathrm{M}}(k) - E_{\mathrm{B}}(k) - \Sigma_{\mathrm{MB}}(k,E)]$ for the unstable $\pi\Delta$, ρN, and σN channels. The self energy $\Sigma_{\mathrm{MB}}(k,E)$ is calculated from a vertex function defining the decay

of the considered unstable particle in the presence of a spectator π or N with a momentum k. For example, we have for the $\pi\Delta$ state,

$$\Sigma_{\pi\Delta}(p,E) = \frac{m_\Delta}{E_\Delta(p)} \int_0^\infty q^2 \mathrm{d}q \frac{M_{\pi\mathrm{N}}(q)}{[M^2_{\pi\mathrm{N}}(q) + p^2]^{1/2}} \times$$
$$\frac{|f_{\Delta \to \pi\mathrm{N}}(q)|^2}{E - E_\pi(p) - [M^2_{\pi\mathrm{N}}(q) + p^2]^{1/2} + \mathrm{i}\epsilon}, \quad (3)$$

where $M_{\pi\mathrm{N}}(q) = E_\pi(q) + E_{\mathrm{N}}(q)$ and $f_{\Delta \to \pi\mathrm{N}}(q)$ defines the decay of the $\Delta \to \pi$N in the rest frame of Δ. The self-energies for ρN and σN channels are similar.

We can split the full partial wave amplitude $T_{\mathrm{MB,M'B'}}(p,p';E)$ into two pieces without introducing any approximation:

$$T_{\mathrm{MB,M'B'}}(p,p';E) = t_{\mathrm{MB,M'B'}}(p,p';E) +$$
$$t^{\mathrm{N}^*}_{\mathrm{MB,M'B'}}(p,p';E). \quad (4)$$

Here the first term is a solution of Eq. (1) but replacing the full transition potential $V_{\mathrm{MB,M'B'}}$ with the meson-exchange potential $v_{\mathrm{MB,M'B'}}$. Therefore $t_{\mathrm{MB,M'B'}}(p,p';E)$ expresses the pure meson-exchange processes and thus is called the meson-exchange amplitude in this paper. The second term describes reaction processes associated with the bare N* states,

$$t^{\mathrm{N}^*}_{\mathrm{MB,M'B'}}(p,p';E) = \sum_{\mathrm{N}_i^*,\mathrm{N}_j^*} \bar{\Gamma}_{\mathrm{MB,N}_i^*}(p;E) \times$$
$$[D(E)]_{i,j} \bar{\Gamma}_{\mathrm{N}_j^*,\mathrm{M'B'}}(p';E), \quad (5)$$

where $\bar{\Gamma}_{\mathrm{N}_j^*,\mathrm{M'B'}}(k;E)$ is the dressed N* $\to$ M'B' vertex function which is defined as

$$\bar{\Gamma}_{\mathrm{N}_j^*,\mathrm{M'B'}}(p,E) = \Gamma_{\mathrm{N}_j^*,\mathrm{M'B'}}(p) +$$
$$\sum_{\mathrm{M''B''}} \int \mathrm{d}q\, q^2 \Gamma_{\mathrm{N}_j^*,\mathrm{M''B''}}(q) G_{\mathrm{M''B''}}(q;E) \times$$
$$t_{\mathrm{M''B'',M'B'}}(q,p;E). \quad (6)$$

The inverse of the propagator of dressed N* states in Eq. (5) is

$$[D^{-1}(E)]_{i,j} = (E - m^0_{\mathrm{N}_i^*})\delta_{i,j} - [M(E)]_{i,j}, \quad (7)$$

where the N* self-energy is defined by

$$[M(E)]_{i,j} = \sum_{\mathrm{MB}} \int_0^\infty q^2 \mathrm{d}q\, \bar{\Gamma}_{\mathrm{N}_j^* \to \mathrm{MB}}(q,E) \times$$
$$G_{\mathrm{MB}}(q,E)\, \Gamma_{\mathrm{MB} \to \mathrm{N}_i^*}(q,E). \quad (8)$$

As for the inclusion of the bare N* states, we impose a condition that the number of the bare N* states included should be as small as possible. This means that if we can explain the data even without some of the bare N* states, then we will take those states out of our model. On the other hand, if we cannot explain some data set with the current model, then we

will try to introduce an additional bare N* state and it may correspond to the new N* state. At present we have introduced 16 number of the bare N* states.

As clearly seen in Eqs. (5)—(8), the bare N* states couple to the meson-baryon continuum through the reaction processes and become resonance states. On the other hand, the meson-exchange amplitude, which describes the pure meson-exchange processes, can also generate the resonance poles dynamically. Our model contains both possibilities.

The MB → M'B' amplitude defined in Eqs. (1)—(8) constitutes a basic ingredient to construct all single and double meson production reactions with the initial πN and $\gamma^{(*)}$N channels. The details of constructing the πN → $\pi\pi$N and $\gamma^{(*)}$N → MB, $\pi\pi$N amplitudes can be found in Refs. [2, 5].

3   Current status of the dynamical coupled-channels analysis at EBAC

3.1 πN → πN scattering

As a steps toward extracting information on the N* states, it is necessary to first determine the hadronic parameters of the EBAC-DCC model. This was accomplished in Ref. [6]. There the SAID πN partial wave amplitudes are considered as the "experimental data" and the hadronic parameters are determined by fitting to them up to $W = 2$ GeV. The numerical fit was performed systematically using the MINUIT library. We refer to this analysis and the obtained parameter set as JLMS in the following.

In Fig. 1 our results of the angular distributions and the polarizations of π^-p → π^-p and π^-p → π^0n calculated from the EBAC-DCC model with the JLMS parameters (solid curves) are compared with the SAID results (da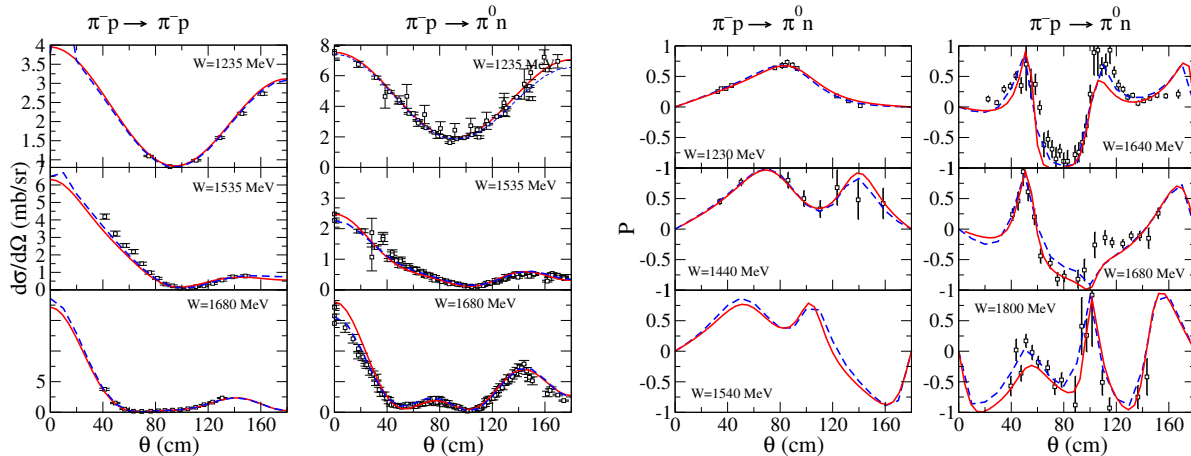shed curves). Our results agree with the SAID results as well as the data. As a next step we plan to improve our hadronic parameters by fitting to the data of these observables.

In Fig. 2, we also present the resulting total cross sections of πN → X (solid curves) and πN → πN (dashed curves) which agree with the data well. The deviation of the πN → X total cross sections above $W = 1.8$ GeV can be understood because in those energy region the multi-pion production reactions, which are not considered in the current EBAC-DCC model, also start to visibly contribute to the total cross sections.

3.2 πN → $\pi\pi$N reaction

With the JLMS parameters obtained from the analysis of the πN scattering, we have calculated cross sections of the πN → $\pi\pi$N reactions in Ref. [5]. Within our model there appears no additional parameters in constructing the πN → $\pi\pi$N amplitude. Thus the results are purely our predictions.

Figure 3 is the resulting total cross sections (solid curves). Without any modifications of the parameters, our results already capture the essential features of the total cross sections up to $W = 2$ GeV. One possible reason for the deviation between our results and the data will be because the πN elastic scattering does not completely fix the parameters associated with the inelastic $\pi\Delta$, ρN, and σN channels. This result indicates that we need a combined, simultaneous analysis of the πN elastic and πN → $\pi\pi$N reactions to construct more complete hadronic amplitudes up to $W = 2$ GeV. In the same figure, we also present the results in which the coupled-channels effect is turned off. We observe that the coupled-channels effect is significant in all W region.
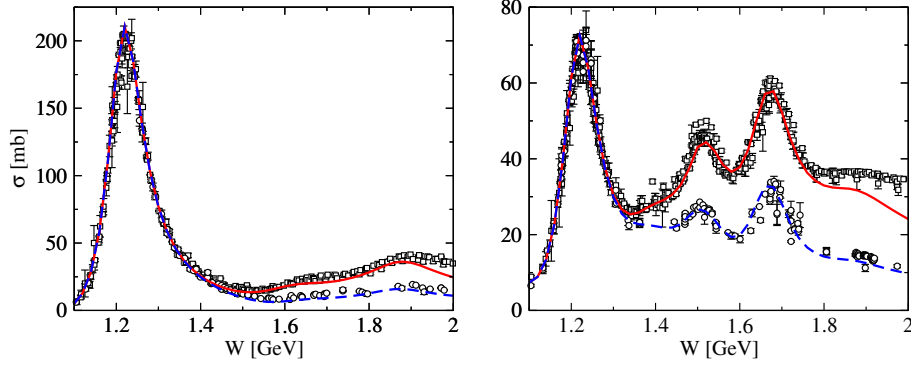

Fig. 1.   Differential cross sections (left) and polarizations (right) of π^-p → π^-p and π^-p → π^0n. The results from EBAC-DCC analysis[6] (solid curves) are compared with those from GWU group[7] (dashed curves).

Fig. 2.   The predicted πN total cross sections from the EBAC-DCC model. (Left panel) The π^+p $\to$ X (solid curve) and π^+p $\to$ π^+p (dashed curve) reactions. (Right panel) The π^-p $\to$ X (solid curve) and π^-p $\to$ π^-p$+\pi^+$n (dashed curve) reactions. The corresponding data to to the solid and dashed curves are presented as open square and open circle, respectively. The data are from Refs. [8, 9].
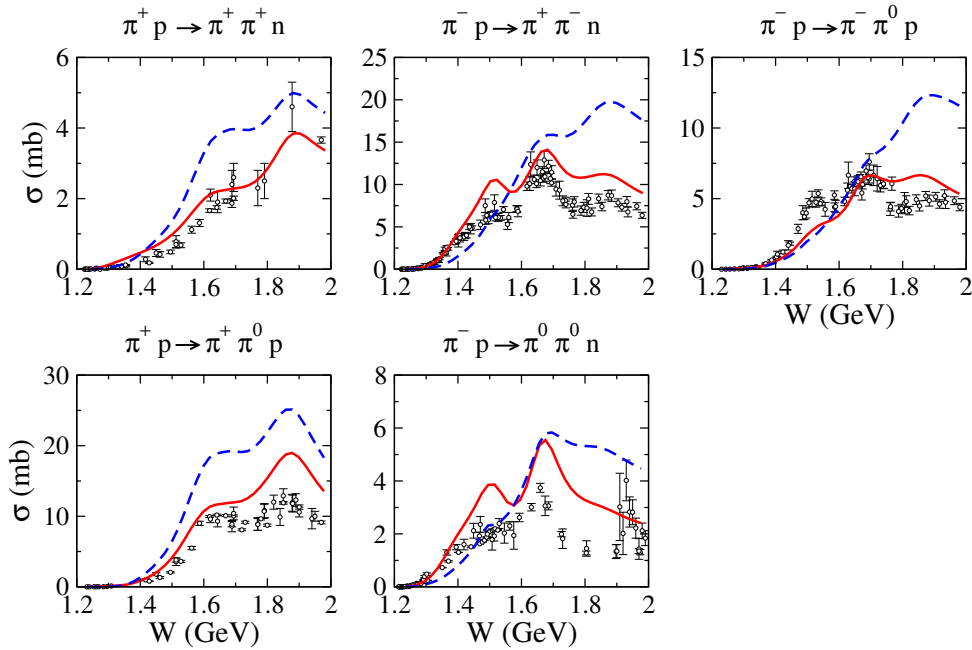

Fig. 3.   The predicted πN $\to$ $\pi\pi$N total cross sections. Solid curves are the full results, and dashed curves are the results in which the coupled-channels effect is turned off. See Ref. [5] for the data references.

In Fig. 4, we present the invariant mass distributions of π^-p $\to$ $\pi^+\pi^-$n. The shape of our results agrees with the data very well except for the $\pi^+\pi^-$ distribution at low W. It is expected that this disagreement with the data provides useful information to refine the parameters associated with the coupling of the low lying N^* states to the ρN and σN channels.

3.3 γN $\to$ πN and eN $\to$ e'πN reactions

The main purpose for analyzing single pion photo- and electro-production reactions is to extract the N-N^* electromagnetic transition form factors. Their precise determination is crucial for understanding the N^* structure because their Q^2 dependence is expected to strongly reflect nature of the N^* structure.

Within the EBAC-DCC model the N-N^* electromagnetic transition form factors are obtained from the dressed γ^*N $\to$ N^* vertex function defined by

$$\bar{\Gamma}_{\gamma^{(*)}N,N^*}(q,Q^2;E) = \Gamma_{\gamma^{(*)}N,N^*}(q,Q^2) +$$

$$\sum_{M''B''} \int dk k^2 v_{\gamma^{(*)}N,M''B''}(q,k,Q^2) \times$$

$$G_{M''B''}(k;E)\bar{\Gamma}_{M''B'',N^*}(k;E), \qquad (9)$$

where $\Gamma_{\gamma^{(*)}N,N^*}(q,Q^2)$ is a bare $\gamma^{(*)}$N $\to$ N^* vertex function and $v_{\gamma^{(*)}N,M''B''}(k,q,Q^2)$ is a meson-exchange $\gamma^{(*)}$N $\to$ M''B'' transition potential.

Our first analysis of the γp $\to$ πN and p(e, e'π)N reactions has been performed up to $W \leqslant 1.6$ GeV in Refs. [12] and [13], respectively. In the analysis

we fixed the hadronic parameters with the JLMS values and varied only the parameters associated with

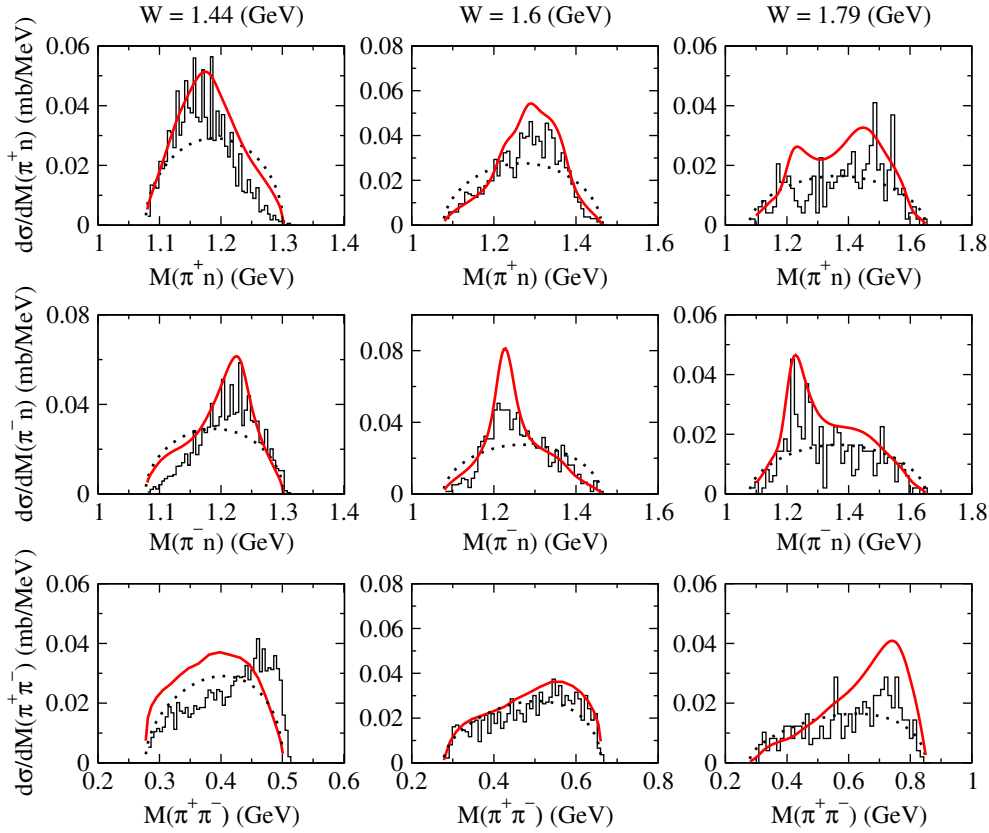electromagnetic interactions, i.e., $\Gamma_{\gamma^{(*)}N,N^*}(q,Q^2)$ and $v_{\gamma^{(*)}N,MB}(k,q,Q^2)$.

Fig. 4.　The predicted invariant mass distributions of the $\pi^-p \rightarrow \pi^+\pi^-n$ reaction at $W = 1.44$, 1.66, and 1.79 GeV. The solid curves are the full results, the dotted curves are the phase-space normalized to the data. The data are from Ref. [10], whose magnitude is determined by normalizing them to the $\pi^-p \rightarrow \pi^+\pi^-n$ total cross sections listed in Ref. [11].

Figures 5 and 6 present our results of the total cross sections of $\gamma p \rightarrow \pi N$ and the five-fold differential cross sections of $p(e,e'\pi)N$ at $Q^2 = 0.4$ $(\text{GeV}/c)^2$, respectively (solid curve). Our results agree with the data very well in the considered energy region up to $W = 1.6$ GeV. We also present that the results in which the coupled-channels effect on the electromagnetic interactions is turned off (dashed curves). As

for the photoproduction reactions, we find that the coupled-channels effect has about 30%—40% of contributions to the cross sections in all W region up to 1.6 GeV. On the other hand, the coupled-channels effect on the electroproduction reactions is still large around $W = 1.2$ GeV but becomes small rapidly at high W for increasing Q^2.
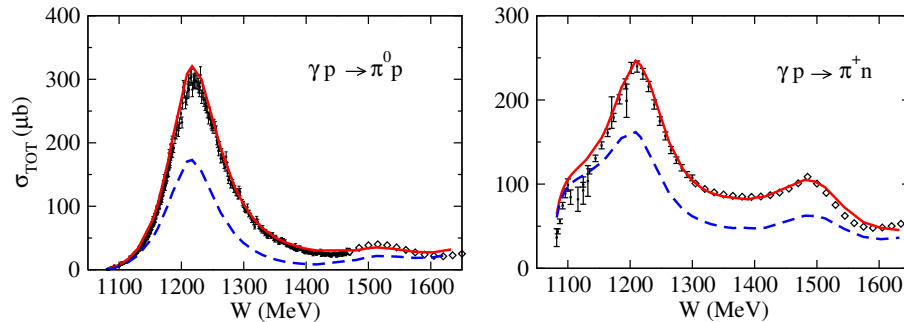

Fig. 5.　The total cross sections of $\gamma p \rightarrow \pi^0 p$ (left) and $\gamma p \rightarrow \pi^+ n$ (right). The solid curves are the full results of EBAC-DCC model; the dashed curves are the results in which the coupled-channels effect in the electromagnetic interactions is turned off (see Ref. [12] for the details).
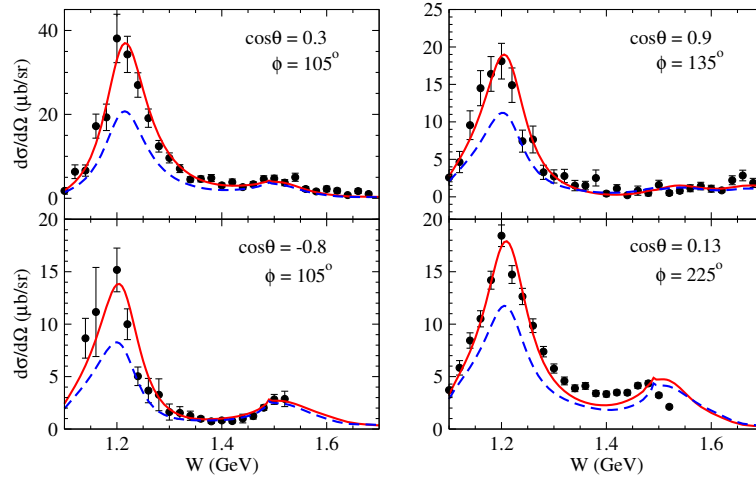
Fig. 6. The five-fold differential cross sections of $p(e, e'\pi^0)p$ (upper panels) and $p(e, e'\pi^+)n$ (lower panels) at $Q^2 = 0.4$ $(\text{GeV}/c)^2$. The meaning of each curve is same as in Fig. 5. The results are taken from Ref. [13].

The resulting G_M^*, G_E^*, and G_C^* form factors of $\gamma^* N \to \Delta(1232)$ and the helicity amplitudes for the higher N^* states evaluated at their Breit-Wigner masses are found in Refs. [12] and [13].

4 Extraction of N^* poles from the constructed scattering amplitudes

Once the scattering amplitude is constructed by analyzing the data of meson production reactions, we can extract various information on the N^* states such as masses, widths, and decay vertex functions. The general scattering theory tells us that the N^* mass and width should be identified with a pole position of the scattering amplitude on the complex energy plane and the N^* decay vertex functions with the residues at the corresponding pole[14—16].

However, the scattering amplitude, which is obtained as a solution of the coupled-channels equation (1), is originally not defined on the complex energy region where the resonance poles exist. To explore the N^* pole positions, we need to make an analytic continuation of the scattering amplitudes. How to perform such analytic continuation both mathematically and numerically is described in detail in Ref. [17]. Therefore here we just present the results of the N^* pole positions extracted from our constructed scattering amplitude.

In Table 1, the extracted N^* pole positions from our current EBAC-DCC model are compared with the PDG values. It is found that most of our results and the PDG values are close to each other. It is noted, however, that we obtain these pole positions from just analyzing the πN scattering and did not try to make our results close to the PDG values at all.

Within our current model, all the extracted N^* states are found to be originated from the bare N^* states [the second term of Eq. (2)] and we find no meson-baryon molecular type of resonances, which is generated dynamically from the pure meson-exchange processes.

Table 1. The resonance pole positions m_R [listed as $(\text{Re } m_R, -\text{Im } m_R)$] extracted from the EBAC-DCC model with the JLMS parameter set are compared with the values of 3- and 4-stars nucleon resonances listed in the PDG[8]. "—" for $P_{33}(1600)$, P_{13} and P_{31} indicates that no resonance pole has been found in the considered complex energy region, $\text{Re}(E) \leqslant 2000$ MeV and $-\text{Im}(E) \leqslant 250$ MeV.

	$m_{N^*}^0$/MeV	m_R/MeV	PDG/MeV
S_{11}	1800	(1540, 191)	(1490 - 1530, 45 - 125)
	1880	(1642, 41)	(1640 - 1670, 75 - 90)
P_{11}	1763	(1357, 76)	(1350 - 1380, 80 - 110)
	1763	(1364, 105)	
	1763	(1820, 248)	(1670 - 1770, 40 - 190)
P_{13}	1711	—	(1660 - 1690, 57 - 138)
D_{13}	1899	(1521, 58)	(1505 - 1515, 52 - 60)
D_{15}	1898	(1654, 77)	(1655 - 1665, 62 - 75)
F_{15}	2187	(1674, 53)	(1665 - 1680, 55 - 68)
S_{31}	1850	(1563, 95)	(1590 - 1610, 57 - 60)
P_{31}	1900	—	(1830 - 1880, 100 - 250)
P_{33}	1391	(1211, 50)	(1209 - 1211, 49 - 51)
	1600	—	(1500 - 1700, 200 - 400)
D_{33}	1976	(1604, 106)	(1620 - 1680, 80 - 120)
F_{35}	2162	(1738, 110)	(1825 - 1835, 132 - 150)
	2162	(1928, 165)	
F_{37}	2138	(1858, 100)	(1870 - 1890, 110 - 130)

We also find in Table 1 that there exist two P_{11}

poles, $(1357, 76)$ and $(1364, 105)$, in the energy region close to the Roper resonance. Here it is noted that recent analysis by the GWU and Jülich groups have also reported the two P_{11} poles in the same energy region[7, 18]. This is quite remarkable because, although the three approaches are based on completely different pictures for the Roper resonance, all of the three present the two poles of the Roper resonance in the same complex energy region after fixing

their model parameters by fitting to the πN scattering data. To conclude whether both of the two poles are the constituents of the Roper resonance, however, we need to make clear how these two poles affect the physics on the real energy axis. This will be accomplished by investigating the magnitude of the residue at the pole positions.

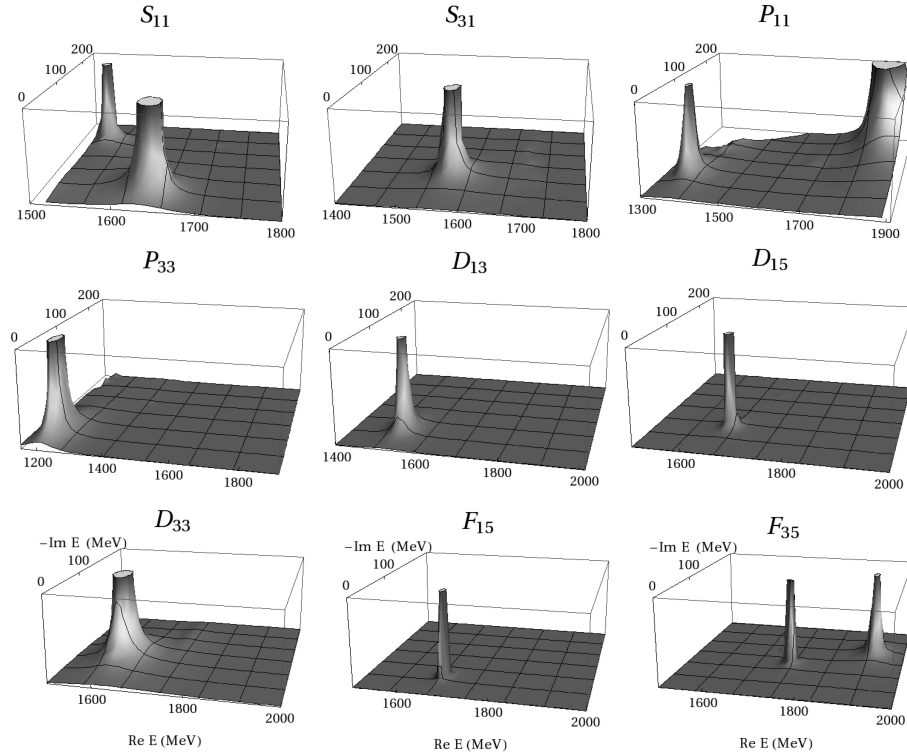In Fig. 7, we present the 3D plots of the N^* pole positions on the complex energy plane.

Fig. 7.   The 3D plots of the N^* pole positions on the complex E plane.

5   Plans for future developments

As a future work, the EBAC program has four main components described in the following subsections.

5.1   Extracting $N^* \to MB$ and $N^* \to \gamma^{(*)}N$ vertex functions

In Sec. 4, we have presented the N^* pole positions extracted from the current EBAC-DCC model. As a next step we will move to the extraction of the $N^* \to MB$ and $N^* \to \gamma^{(*)}N$ vertex functions. As mentioned in Sec. 4, a proper, physically meaningful N^* vertex function is defined by the residue at the corresponding N^* pole, not at the Breit-Wigner mass. Therefore we need to perform an analytic continuation of the scattering amplitude as well as in the case

of pole extraction.

5.2   Analysis of photoproduction reactions and search for new N^* states

We plan to analyze photoproduction reactions of various final states such as KY, ηN, and $\pi\pi$N in the same way as made in the single pion photoproduction reactions. As for these final states, the amount of currently available data of the initial γN are much larger than those of the initial πN. Therefore we will use these photoproduction data to precisely determine the parameters associated with $N^* \to$ KY, $N^* \to \eta$N, and $N^* \to \pi\Delta, \rho$N$, \sigma$N decay vertex functions. Also, the analysis of these reactions is interesting because recent experiments have suggested new N^* states which strongly couple to these reaction channels but not to the dominant πN channel[19, 20]. We could find a possible existence of such new N^*

states from the analysis.

5.3 Developing connection with hadron structure calculations

All N* parameters in the EBAC-DCC model have hitherto been determined by fitting to the data. While this has greatly improved our knowledge of the spectrum, it has not improved our understanding within QCD. For this, it is necessary to develop a method to connect our extracted N* information to the various hadron structure calculations. This is crucial for reaching the final goal of EBAC. Encouragingly, in that connection progress has been made in constituent quark models[21] and Lattice QCD simulations[22, 23].

5.4 Upgrading EBAC-DCC model

In parallel with the above investigations, we keep upgrading EBAC-DCC model. At present the parameters associated with the hadronic interactions are determined by just analyzing the $\pi N \to \pi N$ scattering, and the electromagnetic parameters are determined from the analysis of the single pion photo- and electro-production reactions in which the fixed value of the hadronic parameters are used. However, we have seen that we need a combined, simultaneous analysis of the πN and $\pi\pi N$ channels to obtain more reliable model. In the next step we will refine our model by performing the combined analysis of the

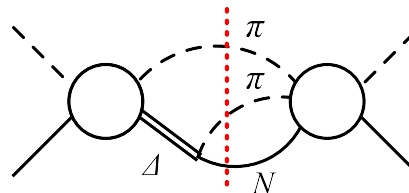$\pi N \to \pi N, \pi\pi N$ and $\gamma N \to \pi N, \pi\pi N$ reactions.

Fig. 8. One example of diagrams including the three-body $\pi\pi N$ unitary cut. The intermediate $\pi\pi N$ state at the red dotted line can be on the mass-shell.

Also, we will incorporate all processes with the $\pi\pi N$ 3-body unitary cut. Some of the processes as shown in Fig. 8 have not been included in our current model. Such processes could be important for the meson production reactions up to 2 GeV. As far as we know, such complete treatment of the three-body unitary cut has never been done before in the N* study, and thus this improvement will make our model unique from other dynamical models.

References

1 Burkert V D, Lee T S H. Int. J. Mod. Phys. E, 2004, **13**: 1035
2 Matsuyama A, Sato T, Lee T S H. Phys. Rept., 2007, **439**: 193
3 Sato T, Lee T S H. Phys. Rev. C, 1996, **54**: 2660
4 Sato T, Lee T S H. arXiv:0902.3653 [nucl-th]
5 Kamano H, Juliá-Díaz B, Lee T S H, Matsuyama A, Sato T. Phys. Rev. C, 2009, **79**: 025206
6 Juliá-Díaz B, Lee T S H, Matsuyama A, Sato T. Phys. Rev. C, 2007, **76**: 065201
7 Arndt R A, Briscoe W J, Strakovsky I I, Workman R L. Phys. Rev. C, 2006, **74**: 045205
8 Amsler C et al (Particle Data Group). Phys. Lett. B, 2008, **667**: 1
9 CNS Data Analysis Center (GWU). http://gwdac.phys.gwu.edu
10 Arndt R A. private communications
11 Manley D M, Arndt R A, Goradia Y, Teplitz V L. Phys. Rev. D, 1984, **30**: 904
12 Juliá-Díaz B, Lee T S H, Matsuyama A, Sato T, Smith L C.
Phys. Rev. C, 2008, **77**: 045205
13 Juliá-Díaz B, Kamano H, Lee T S H, Matsuyama A, Sato T, Suzuki N. Phys. Rev. C, 2009, **80**: 025207
14 Goldberger M L, Watson K M. Collision Theory. Dover, 2004
15 de la Madrid R, Gadella M. Am. J. Phys, 2002, **70**: 626
16 Bohm R A, Sato Y. Phys. Rev. D, 2005, **71**: 085018
17 Suzuki N, Sato T, Lee T S H. Phys. Rev. C, 2009, **79**: 025205
18 Doring M, Hanhart C, Huang F, Krewald S, Meißner U-G. arXiv:0903.4337 [nucl-th]
19 McNabb J W C et al (CLAS collaboration). Phys. Rev. C, 2004, **69**: 042201
20 Sumihama M et al (LEPS collaboration). Phys. Rev. C, 2006, **73**: 035214
21 Aznauryan I G et al (CLAS collaboration). Phys. Rev. C, 2008, **78**: 045209
22 Alexandrou C, de Forcrand Ph, Negele W J, Schroers W, Tsapalis A. Phys. Rev. Lett., 2005, **94**: 021601
23 Lin H W, Cohen S D, Edwards R G, Richards D G. Phys. Rev. D, 2008, **78**: 114508